IEEE Access
Multidisciplinary | Rapid Review | Open Access Journal

Received March 28, 2020, accepted April 14, 2020, date of publication April 20, 2020, date of current version May 4, 2020.

Digital Object Identifier 10.1109/ACCESS.2020.2988800

Inverted Pendulum Nonlinear Controllers Using Two Reaction Wheels: Design and Implementation

JOÃO FRANCISCO SILVA TRENTIN[1], SAMUEL DA SILVA[1], JEAN MARCOS DE SOUZA RIBEIRO[2], AND HANSPETER SCHAUB[3]

[1]Departamento de Engenharia Mecânica, Faculdade de Engenharia de Ilha Solteira, Universidade Estadual Paulista (UNESP), Ilha Solteira 15385-000, Brazil
[2]Departamento de Engenharia Elétrica, Faculdade de Engenharia de Ilha Solteira, Universidade Estadual Paulista (UNESP), Ilha Solteira 15385-000, Brazil
[3]Colorado Center for Astrodynamics Research, Department of Aerospace Engineering Sciences, University of Colorado Boulder, Boulder, CO 80303, USA

Corresponding author: João Francisco Silva Trentin (joao.trentin@unesp.br)

This work was supported by the São Paulo Research Foundation (FAPESP) under Grant 2018/13751-8, and in part by the National Council of Technological and Scientific Development (CNPq) under Grant 306526/2019-0.

ABSTRACT Reaction wheels have been extensively used to control and stabilize a wide range of applications due to the angular momentum exchange that they provide to mechanical systems. However, there exist several limitations associated with actuator saturation and the presence of singularities that lead towards the use of different controllers and devices. Recently, a new and unusual configuration using two reaction wheels was proposed and illustrated in an inverted pendulum to drive and control it using a simple and well-known PID controller. In this context, this paper improves the previous results on the same system by proposing two more sophisticated nonlinear controllers: a nonlinear proportional-derivative and a sliding mode controller. The proof of the stability of each controller is also provided, and the asymptotic stability is proven. A friction model is experimentally updated into the differential equations of the pendulum and also included for the controllers designing. A real-time application verifies the performance of the controllers using low-cost hardware. Results based on the analysis of different performance indices highlight the improvement of applying these two nonlinear control techniques comparing to the previous paper using this configuration of actuators.

INDEX TERMS Inverted pendulum, low-cost hardware, reaction wheels, sliding mode control.

I. INTRODUCTION

Inverted pendulum models such as the wheeled inverted pendulum, the pendulum and a cart system, and the reaction wheel pendulum, among others, have been subject to studies for decades, helping to develop new control strategies or even describing the dynamics of real-world mechanisms [1]–[5]. Other inverted pendulum-like systems have been studied recently. Owczarkowski *et al.* [6] investigated the control of a real bicycle robot which has its balance controlled by a reaction wheel pendulum, where a combination of feedback-linearization-based techniques and robust LQR control laws was carried out. Moreover, the studies of unicycles were also conducted, where Jin *et al.* [7] used the gyroscopic precession of two gyroscopes to provide lateral balance to the system. Neves *et al.* [8] designed a robust controller that minimized the $\mathcal{H}_2$ system norm considering parametric uncertainties in the poly-topic domain for a reaction wheel unicycle, and the controller performance was verified experimentally. A ball-bot system, a pendulum balanced on a ball, has also attracted attention in the past few years [9]–[11]. This system consists of an inverted pendulum rolling on a sphere and can be controlled by its Omni-wheels [10] or using reaction wheels [11]. Sekhar *et al.* [11] derived a mathematical model using Lagrangian mechanics, where it included reaction wheels to control the ball-bot system. PID and LQR controllers were designed to control the system with or without the reaction wheels to compare the performances. Furthermore, Lima *et al.* [10] verified experimentally a LMI based robust $\mathcal{H}_2$ controller for such a system. Also, the majority of these inverted pendulum-like systems are nonlinear and under-actuated, which makes their control

The associate editor coordinating the review of this manuscript and approving it for publication was Nasim Ullah.

and stabilization more complicated [12]. Thus, the problem of balancing inverted pendulum systems is of great importance for control and robotic communities.

Trentin *et al.* [13] suggested an unusual and new pendulum configuration where instead of using only a reaction wheel to drive and control a pendulum in the inverted position, it uses two. A simple PID controller was designed to evaluate the difference of actuating an inverted pendulum with one or two actuators. This system may attract attention for many reasons, ranging from academic and pedagogic purposes to the development of new control techniques. It is also interesting that one can use one reaction wheel or both to drive the pendulum to the inverted position.

There is a large variety of control techniques to be applied to stabilize inverted pendulums. The present paper intends to investigate the use of two nonlinear control techniques, one Lyapunov-based and other based on variable structure control (VSC), to be applied in the same configuration that we proposed in Trentin *et al.* [13]. The Lyapunov direct method can provide a helpful tool to analyze the stability of dynamical systems. From this method, it is possible to propose energy-like functions that must be positive definite with its derivative being at least negative semi-definite [14]–[17]. Therefore, this function will be a Lyapunov function and the stability analysis of the problem can be carried out.

The variable structure control is an advanced nonlinear control strategy that has provided adequate means to design robust state feedback controllers. The aim is to obtain the desired plant behavior, changing its structure automatically on reaching a switching surface. It is an efficient control strategy that is used to a broad class of both nonlinear and linear systems subject to external disturbances and modeling uncertainty [18]–[20]. The controller structure is changed by using a high-speed switching feedback control. The switching feedback control law drives the trajectory of the system onto a specified and user-chosen surface, which is termed the sliding surface or the switching surface and maintains the trajectory on this sliding surface for all subsequent time [18], [20], [21]. The primary mode of variable structure control operation is sliding mode control, which includes excellent properties, such as low sensitivity to plant parameter uncertainty, rejection of a particular class of external disturbances, reduced-order modeling of plant dynamics, and finite-time convergence [18]–[22].

The basic principle of VSC theory is to design a switching surface, which has the desired behavior of the states, and a control law that brings the states to that surface. The advantage is that once the system's states reach the switching surface, the system operation mode depends only on the equation of the switching surface designed, regardless of the parameters of the system, even if the system parameters have a change [18], [20]. Therefore, the VSC theory can overcome the invariance of uncertain parameters such as disturbance and perturbation of parameters, and can reduce the order of the system and the algorithm is simple and easy to realize [23].

Although the theory of variable structure systems has undergone extensive and detailed studies in the control community [23]–[25]. In recent years, researches on VSC theory has been successfully applied to a wide variety of practical systems, such as satellite and spacecraft attitude control [26]–[30], power model [31], cranes [32], [33], quadrotors [34] and robot control [35]–[37]. The variable structure control technique also has wide application in advanced microprocessor technology of the on-line control of dynamic systems, for example, robotic manipulators, heat processes, electro-pneumatic system [24]. Additionally, for inverted pendulum systems, Riachy *et al.* [38] designed a second-order sliding mode controller for an inverted pendulum under uncertainty conditions. Furthermore, Wang [39] carried out the stabilization and tracking control using sliding modes of an X-Z inverted pendulum that can move combining vertical and horizontal forces. Iriarte *et al.* [40] presented a second-order sliding mode tracking controller for the reaction wheel pendulum. Adhikary and Mahanta [41] proposed an integral back-stepping sliding mode controller for the swing-up and stabilization of the pendulum and a cart system. Guo *et al.* [42] carried out the design and implementation of a sliding mode controller for the wheeled inverted pendulum.

Thereby, the main contribution of this paper is to describe new control realizations regarding the pendulum with two reaction wheels to improve the performance comparing with our previous paper [13]. This paper illustrates the design of two nonlinear controllers for the two reaction wheels pendulum (2-RWP). The first one designed is a classical nonlinear proportional-derivative controller derived from the Lyapunov stability theory. The proof of stability is provided using the higher-order derivatives of the Lyapunov function candidate, where the asymptotic stability is proven. Additionally, considering that many parameters of the plant are known with limited accuracy, a sliding mode controller is also designed for this different pendulum configuration. The new results obtained experimentally using low-cost hardware are compared to established ones. Moreover, the way that the plant was manufactured using DC motors without encoders makes it impossible to know many of the states of the reaction wheels. This was taken into account in the design of the controllers, which have to be able to overcome this practical challenge.

This paper is organized as follows. Primarily, section II describes the model of the pendulum with two reaction wheels and the experimental characterization of the pendulum friction. Subsequently, section III presents a Lyapunov-based proportional-derivative controller. The design of the sliding mode controller for the 2-RWP is carried out in section IV in which the stability analysis assures asymptotically stability. Furthermore, section V exhibits the description of the experimental set-up used for the tests of the nonlinear controllers in real-time, showing the low-cost hardware. Afterwards, the results obtained using the nonlinear controllers are shown in section VI. They are compared to the previous one highlighting the improvement of using the

two control techniques proposed in this paper. Finally, the conclusions are carried out.

II. MODEL OF THE TWO REACTION WHEELS PENDULUM

The pendulum with two reaction wheels is presented in Fig. 1. The complete model of this unusual pendulum configuration was carried out in [13], where θ describes the pendulum motion, α the motion of *reaction wheel 1* and β the motion of the *reaction wheel 2*.

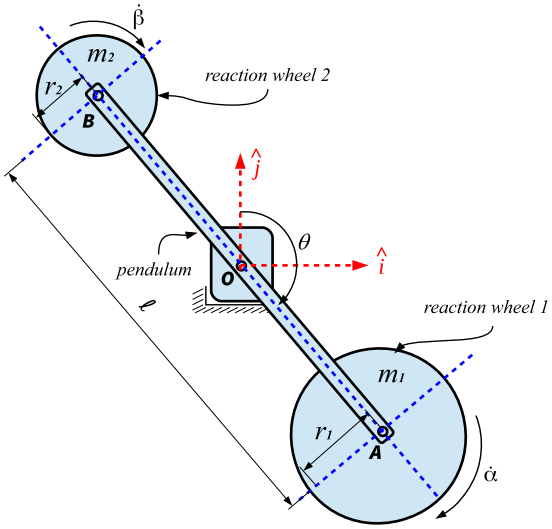

FIGURE 1. Two reaction wheels pendulum [13].

The equation of motion of the 2-RWP is given by:

$$I^O_{zeq}\ddot{\theta} + I^O_{zw1}\ddot{\alpha} + I^O_{zw2}\ddot{\beta} = (m_1 - m_2)g\frac{\ell}{2}\sin\theta \tag{1}$$

where $I^O_{zeq} = \frac{1}{12}m_p\ell^2 + \frac{1}{2}\left(m_1 r_1^2 + m_2 r_2^2\right) + \frac{1}{4}\left(m_1\ell^2 + m_2\ell^2\right)$ is the moment of inertia of the pendulum and both reaction wheels computed relatively to the fixed point O using Steiner's Theorem, m_p is the pendulum mass, ℓ is the pendulum length, g is the acceleration of gravity, and θ describes the angular position of the pendulum. The moments of inertia of each reaction wheel are $I^O_{zw1} = \frac{1}{2}m_1 r_1^2 + \frac{1}{4}m_1\ell^2$ and $I^O_{zw2} = \frac{1}{2}m_2 r_2^2 + \frac{1}{4}m_2\ell^2$, respectively. They were also calculated relatively to the fixed point O. $\ddot{\theta}$ is the angular acceleration of the pendulum, $\ddot{\alpha}$ is the angular acceleration of *reaction wheel 1*, $\ddot{\beta}$ is the angular acceleration of *reaction wheel 2*, m_1 and m_2 are the masses, and r_1 and r_2 are the radii of the reaction wheels 1 and 2, respectively.

Additionally, the motor torques for each reaction wheel are:

$$T_1 = I^A_{zw1}\ddot{\theta} + I^A_{zw1}\ddot{\alpha} \tag{2}$$
$$T_2 = I^B_{zw2}\ddot{\theta} + I^B_{zw2}\ddot{\beta} \tag{3}$$

where with respect to the point A, the moment of inertia of the *reaction wheel 1* is $I^A_{zw1} = \frac{1}{2}m_1 r_1^2$, and the moment of inertia of *reaction wheel 2* is $I^B_{zw2} = \frac{1}{2}m_2 r_2^2$ relatively to the fixed point B. The parameters used for simulations were $m_1 = 0.21$ kg, $r_1 = 0.11$ m, $m_2 = 0.13$ kg, $r_2 = 0.1$ m, $m_p = 0.16$ kg and $\ell = 0.5$ m. These parameters were obtained from the experimental device. Equations (1), (2) and (3) describe the motion of the 2-RWP.

The torques T_1 and T_2 are provided by DC motors coupled to the reaction wheels, whose equations are given by:

$$T_1 = V_\alpha\frac{K_t}{R_a} - \frac{K_t K_v}{R_a}\dot{\alpha} \tag{4}$$
$$T_2 = V_\beta\frac{K_t}{R_a} - \frac{K_t K_v}{R_a}\dot{\beta} \tag{5}$$

And equations (4) and (5) can be rearranged in such manner that they will provide the necessary voltage for each DC motor based on the motor torques:

$$V_\alpha = T_1\frac{R_a}{K_t} + K_v\dot{\alpha} \tag{6}$$
$$V_\beta = T_2\frac{R_a}{K_t} + K_v\dot{\beta} \tag{7}$$

where R_a is the armature resistance, K_t is the motor torque constant, and K_v is the back electromotive force constant.

From the experimental characterization of the DC motor already presented in [13], where a first-order transfer function represents the DC motor coupled to the reaction wheel relating the angular velocity of the reaction wheel with the voltage applied to the DC motor, the values obtained for the stationary gain and for the time constant were: $K = 54.62$ Vs/rad and $\tau = 5.88$ s. Considering these values and the moment of inertia of each reaction wheel is possible to find that $R_a = 1.06\,\Omega$, $K_t = 0.0063$ Vs/rad and $K_v = 0.0063$ Nm/A.

A. EXPERIMENTAL CHARACTERIZATION OF THE PENDULUM FRICTION

It is essential to highlight that the pendulum built for the experimental tests has some construction imperfections and presents a nonlinear behavior regarding its friction. The pendulum angular motion has small velocities for which is difficult to model the effect of friction [43]. Therefore, it is imperative to include such a phenomenon in the model of the pendulum with two reaction wheels. The model must consider the contributions of Coulomb and viscous friction to be able to represent this phenomenon, and it is described by:

$$T_{fr} = \text{sgn}(\dot{\theta})\left(C_v|\dot{\theta}| + C_c\right) \tag{8}$$

where C_v is the coefficient of viscous friction and C_c the Coulomb friction value. The parameters of this friction model were identified, and the model was included in the equation of motion of the 2-RWP presented in (1). Regarding the identification of the model, the pendulum was released from $\theta = 90$ degrees so that the friction behavior could be observed until the pendulum stopped in the stable equilibrium point, the downward position. Fig. 2 presents the experimental result of releasing the pendulum and waiting for it to stop and compares this result with the 2-RWP equation of motion with the friction model included given by:

$$I^O_{zeq}\ddot{\theta} + I^O_{zw1}\ddot{\alpha} + I^O_{zw2}\ddot{\beta} = (m_1 - m_2)g\frac{\ell}{2}\sin\theta - T_{fr} \tag{9}$$

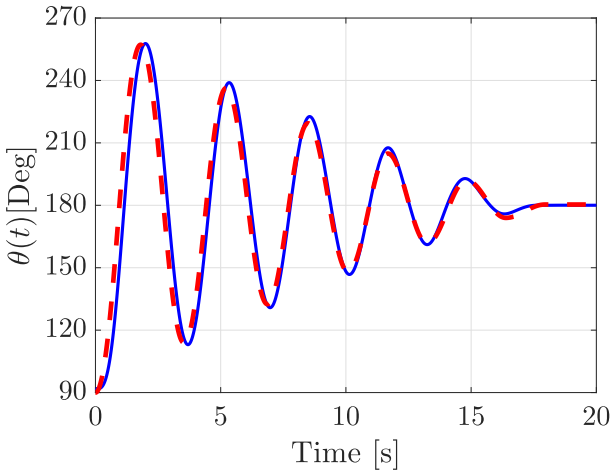

FIGURE 2. Identification of the friction of the 2-RWP. - - - indicates numerical result and ___ the experimental result.

This model has a very close fit to the experimental result, where $C_v = 0.0031$ Nms/rad and $C_c = 0.011$ Nm. Also, the friction model used here, composed by viscous and Coulomb friction contribution, is trendy in the literature [43]. Moreover, this has not been considered in our previous paper [13], and the friction contribution is significant to be identified and included in the design of the controllers once it has a strong nonlinear behavior and this could influence in the performance of the controllers.

III. DESIGN OF A NONLINEAR PROPORTIONAL-DERIVATIVE CONTROLLER

This section presents the design of a proportional-derivative controller using a Lyapunov-based approach and also considering the nonlinear friction model of the 2-RWP. It is necessary to select an energy-like candidate to be a Lyapunov function to design the feedback control law:

$$\mathcal{V}(\delta\theta, \delta\dot{\theta}) = I^O_{zeq}\frac{\delta\dot{\theta}^2}{2} + k_p\frac{\delta\theta^2}{2} \tag{10}$$

where $\delta\dot{\theta} = \dot{\theta} - \dot{\theta}_d$, $\delta\theta = \theta - \theta_d$ and k_p is a positive feedback gain. To the system to be stable, the derivative of the Lyapunov candidate function must be at least negative semi-definite. The derivative of the candidate for Lyapunov function is given by:

$$\dot{\mathcal{V}}(\delta\theta, \delta\dot{\theta}) = \delta\dot{\theta}\left(I^O_{zeq}\delta\ddot{\theta} + k_p\delta\theta\right) \tag{11}$$

In this way, $\dot{\mathcal{V}}(\delta\theta, \delta\dot{\theta})$ is set to be equal to a negative semi-definite function, in this case:

$$\dot{\mathcal{V}}(\delta\theta, \delta\dot{\theta}) = \delta\dot{\theta}\left(I^O_{zeq}\delta\ddot{\theta} + k_p\delta\theta\right) = -k_d\delta\dot{\theta}^2 \tag{12}$$

where k_d is a positive gain. It is possible to obtain the following stable closed-loop dynamical system to develop the derivative of the Lyapunov candidate function:

$$I^O_{zeq}\ddot{\theta} - I^O_{zeq}\ddot{\theta}_d + k_p\delta\theta + k_d\delta\dot{\theta} = 0 \tag{13}$$

To find the control law, it is necessary to substitute the system motion equation (9) into the closed-loop system presented in (13), yielding:

$$-I^O_{zw1}\ddot{\alpha} - I^O_{zw2}\ddot{\beta} + (m_1 - m_2)g\frac{\ell}{2}\sin\theta - T_{fr} + \\ - I^O_{zeq}\ddot{\theta}_d + k_p\delta\theta + k_d\delta\dot{\theta} = 0 \tag{14}$$

and rearranging, we obtain the control law for the 2-RWP:

$$\left[I^O_{zw1}\ I^O_{zw2}\right]\left\{\begin{array}{c}\ddot{\alpha}\\ \ddot{\beta}\end{array}\right\} = (m_1 - m_2)g\frac{\ell}{2}\sin\theta - T_{fr} + \\ - I^O_{zeq}\ddot{\theta}_d + k_p\delta\theta + k_d\delta\dot{\theta} \tag{15}$$

Usually, to guarantee the asymptotic stability of a system, the candidate for Lyapunov function $\mathcal{V}(\delta\theta, \delta\dot{\theta})$ must be positive definite, whereas its derivative $\dot{\mathcal{V}}(\delta\theta, \delta\dot{\theta})$ must be negative definite. This is a sufficient condition but not a necessary one. If the Lyapunov function derivative is only negative semi-definite, it is still possible for a dynamical system to be asymptotically stable [17]. The theorem enunciated below, introduced by Mukherjee and Chen [44], provides the necessary conditions to prove asymptotic stability when the Lyapunov function derivative is only semi-definite $\dot{\mathcal{V}}(\delta\theta, \delta\dot{\theta}) \leqslant 0$ by investigating the higher order derivatives of the Lyapunov functions [44]–[46].

Theorem: Assume there exists a Lyapunov function $\mathcal{V}(\boldsymbol{x})$ of the dynamical system $\dot{\boldsymbol{x}} = \boldsymbol{f}(\boldsymbol{x})$. Let $\boldsymbol{\Omega}$ be the non-empty set of state space vectors such that

$$\boldsymbol{x} \in \boldsymbol{\Omega} \Rightarrow \dot{\mathcal{V}}(\boldsymbol{x}) = 0$$

If the first $k-1$ derivatives of $\mathcal{V}(\boldsymbol{x})$, evaluated on the set $\boldsymbol{\Omega}$, are zero

$$\frac{\mathrm{d}^i\mathcal{V}(\boldsymbol{x})}{\mathrm{d}t^i} = 0 \quad \forall\boldsymbol{x} \in \boldsymbol{\Omega} \quad i = 1, 2, \ldots, k-1$$

and the k-th derivative is negative definite on the set $\boldsymbol{\Omega}$

$$\frac{\mathrm{d}^k\mathcal{V}(\boldsymbol{x})}{\mathrm{d}t^k} < 0 \quad \forall\boldsymbol{x} \in \boldsymbol{\Omega}$$

then the system $\boldsymbol{x}$ is asymptotically stable if k is an odd number.

The proof of the theorem is provided in [44]. Thereby, to find out which kind of stability the proposed control law guarantees, the higher-order derivatives of the candidate to the Lyapunov function are analyzed. Starting with the second derivative of the candidate to Lyapunov function, presented in (16), none information is obtained.

$$\ddot{\mathcal{V}}(\delta\theta, \delta\dot{\theta}) = -2k_d\delta\dot{\theta}\delta\ddot{\theta}; \quad \ddot{\mathcal{V}}(\delta\theta, \delta\dot{\theta} = 0) = 0 \tag{16}$$

Thus, it is necessary to analyse the third derivative of $\mathcal{V}(\delta\theta, \delta\dot{\theta})$:

$$\dddot{\mathcal{V}}(\delta\theta, \delta\dot{\theta}) = -2k_d\delta\ddot{\theta}^2 - 2k_d\delta\dot{\theta}\delta\dddot{\theta} \tag{17}$$

considering that $\delta\dot{\theta} = 0$:

$$\dddot{\mathcal{V}}(\delta\theta, \delta\dot{\theta} = 0) = -2k_d\delta\ddot{\theta}^2 \tag{18}$$

and analyzing it when $\dot{\mathcal{V}}(\delta\theta, \delta\dot{\theta} = 0)$, yields:

$$\delta\ddot{\theta} = -k_p \delta\theta \tag{19}$$

Substituting the result presented in (19) into (18):

$$\ddot{\mathcal{V}}(\delta\theta, \delta\dot{\theta} = 0) = -2k_d k_p^2 \delta\theta^2 < 0 \tag{20}$$

The third derivative of $\mathcal{V}(\delta\theta, \delta\dot{\theta})$ is negative definite in terms of $\delta\dot{\theta}$, and because the first non-zero $\mathcal{V}$ derivative is of odd order, the control law is asymptotically stable.

IV. DESIGN OF A SLIDING MODE CONTROLLER

This section presents the design of a sliding mode controller for the 2-RWP to evaluate how the results of a simple approach to robust control would perform when compared with other control techniques. It is crucial to specify a sliding surface or to choose a sliding function to design a controller using sliding modes [20]. The dynamic regime of this surface is chosen in such a way that all the trajectories within this surface converge to the desired value [18]–[20]. However, in the design of a sliding mode controller, this surface must be chosen in a way where the dynamic of the system become stable and, therefore, a control law must be defined where all trajectories are driven to the sliding surface. For the design of the sliding mode controller, we used a sliding function instead of a surface, since the majority of the states of the experimental 2-RWP are unknown. Thereby, the controller was designed using the known states. The tracking error, defined as $e = \theta - \theta_d$, is associated to the desired trajectory and the sliding function is defined by equation $\sigma(e, t) = 0$:

$$\sigma(e, t) = \dot{e} + \gamma e \tag{21}$$

where γ is a positive constant associated with the closed-loop bandwidth [18]. Equation (21) represents a straight line of sliding in the error configuration space. The sliding function defined must have its values tending to zero, to converge with a finite time interval. From the sliding surface presented in (21), its derivative yields:

$$\dot{\sigma} = \ddot{e} + \gamma\dot{e} \equiv \ddot{\theta} - \ddot{\theta}_d + \gamma\dot{e} \tag{22}$$

Here, it is necessary to select a candidate to be a Lyapunov function $\mathcal{V}(\sigma)$ being positive definite, and that has a definite negative derivative, where a possible one is:

$$\mathcal{V}(\sigma) = \frac{1}{2}\sigma^2 \tag{23}$$

With the presented candidate for Lyapunov function, the sliding mode will exist, and the system will be stable if $\dot{\mathcal{V}}(\sigma)$ is negative definite:

$$\dot{\mathcal{V}}(\sigma) = \sigma\dot{\sigma}, \quad \sigma \neq 0 \tag{24}$$

The motion equation of 2-RWP including the friction term, presented in (9), can be rearranged and substituted into the derivative of the sliding function in (22):

$$\dot{\sigma} = \frac{(m_1 - m_2) g \frac{\ell}{2} \sin\theta}{I^O_{zeq}} - \frac{I^O_{zw1}}{I^O_{zeq}}\ddot{\alpha} - \frac{I^O_{zw2}}{I^O_{zeq}}\ddot{\beta} + - \frac{T_{fr}}{I^O_{zeq}} - \ddot{\theta}_d + \gamma\dot{e} \tag{25}$$

which leads to:

$$\dot{\sigma} = \frac{(m_1 - m_2) g \frac{\ell}{2} \sin\theta}{I^O_{zeq}} - \underbrace{\begin{bmatrix} \frac{I^O_{zw1}}{I^O_{zeq}} & \frac{I^O_{zw2}}{I^O_{zeq}} \end{bmatrix} \begin{Bmatrix} \ddot{\alpha} \\ \ddot{\beta} \end{Bmatrix}}_{u} + - \frac{T_{fr}}{I^O_{zeq}} - \ddot{\theta}_d + \gamma\dot{e} \tag{26}$$

The control law u can be adopted as:

$$u = \begin{bmatrix} \frac{I^O_{zw1}}{I^O_{zeq}} & \frac{I^O_{zw2}}{I^O_{zeq}} \end{bmatrix} \begin{Bmatrix} \ddot{\alpha} \\ \ddot{\beta} \end{Bmatrix} = \frac{(m_1 - m_2) g \frac{\ell}{2} \sin\theta}{I^O_{zeq}} + - \frac{T_{fr}}{I^O_{zeq}} - \ddot{\theta}_d + \gamma\dot{e} + \eta\,\mathrm{sgn}(\sigma) \tag{27}$$

The control law proposed in equation (27) can be substituted into the derivative of the sliding function shown in (26) resulting:

$$\dot{\sigma} = -\eta\,\mathrm{sgn}(\sigma) \tag{28}$$

The result presented in (28) is substituted into the derivative of the candidate for the Lyapunov function given in equation (24) to prove that the selected function is a Lyapunov function with a definite negative derivative:

$$\dot{\mathcal{V}}(\sigma) = \sigma\,(-\eta\,\mathrm{sgn}(\sigma)) = -\eta|\sigma| < 0, \quad \sigma \neq 0 \tag{29}$$

where η is an arbitrary positive constant and $\mathrm{sgn}(\sigma)$ is a signal function defined as:

$$\mathrm{sgn}(\sigma) = \begin{cases} 1 & \text{if } \sigma > 0 \\ 0 & \text{if } \sigma = 0 \\ -1 & \text{if } \sigma < 0 \end{cases} \tag{30}$$

From a practical point of view, a sliding mode cannot exist because this would require that the controller switches at an infinite frequency. In the presence of switching imperfections, the discontinuity in controller feedback produces a particular behavior known as chattering [18]. Slotine and Li [18] proposed to smooth signal function $\mathrm{sgn}(\sigma)$ used in the control law to avoid chattering. So, a boundary layer around the sliding function is established. Thus, to restrain the chattering phenomenon, a saturated function $\mathrm{sat}(\sigma)$ is adopted instead of signal function $\mathrm{sgn}(\sigma)$:

$$\mathrm{sat}(\sigma) = \begin{cases} 1 & \text{if } \sigma > \Delta \\ k\sigma & \text{if } |\sigma| \leq \Delta, \quad k = \frac{1}{\Delta} \\ -1 & \text{if } \sigma < -\Delta \end{cases} \tag{31}$$

Thus, employing the saturation function in the adopted control law that was presented in (27) and rewriting it:

$$u = \begin{bmatrix} \frac{I^O_{zw1}}{I^O_{zeq}} & \frac{I^O_{zw2}}{I^O_{zeq}} \end{bmatrix} \begin{Bmatrix} \ddot{\alpha} \\ \ddot{\beta} \end{Bmatrix} = \frac{(m_1 - m_2) g \frac{\ell}{2} \sin\theta}{I^O_{zeq}} + - \frac{T_{fr}}{I^O_{zeq}} - \ddot{\theta}_d + \gamma\dot{e} + \eta\,\mathrm{sat}(\sigma) \tag{32}$$

Since the sliding mode control law can be separated into two main components, the equivalent and the switching parts, equation (32) can be written as:

$$u = u_{eq} + u^{\pm} \tag{33}$$

where

$$u_{eq} = \frac{(m_1 - m_2)g\frac{\ell}{2}\sin\theta}{I^O_{zeq}} - \frac{T_{fr}}{I^O_{zeq}} - \ddot{\theta}_d + \gamma\dot{e} \tag{34}$$

and

$$u^{\pm} = \eta \text{sat}(\sigma) \tag{35}$$

The switching component of the control law ($u^{\pm}$) takes the system to the sliding function, and the equivalent component (u_{eq}) is important when the system is sliding ($u^{\pm} = 0$), since this component is responsible for driving the states to the equilibrium point.

V. EXPERIMENTAL DESCRIPTION

This section presents the experimental device used for the tests and explains how the real-time nonlinear controllers work using the low-cost hardware proposed. Fig. 3 depicts the 2-RWP constructed for experimental tests. The set-up built has a Vishay spectral multi-turn potentiometer model 533 used to measure the pendulum angle. Here, an encoder could be used; however, a secondary objective of the paper is to analyze the performance of the low-cost hardware for the application of nonlinear controllers. To each reaction wheel, a DC motor Akiyama model AK555/390ML 12S18200C was coupled. It operates with a nominal voltage of 12 V.

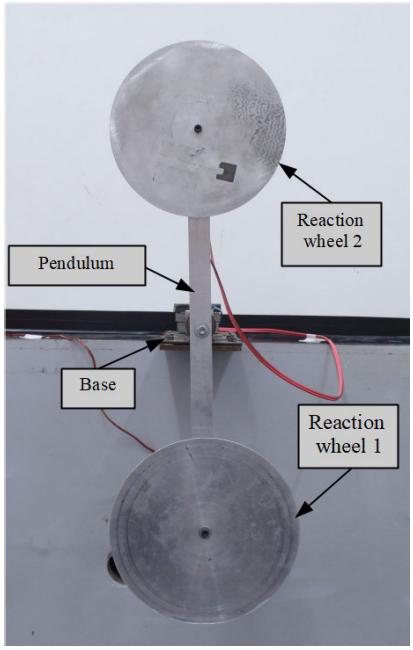

FIGURE 3. Two reaction wheels pendulum built for the experimental tests [13].

Additionally, an Arduino Uno prototype platform that has a micro-controller was used to program the control laws for the real-time application. A two-relay module Shun Yu, model BTE13-00, and two PWM control boards complete the necessary hardware to run the tests. This hardware costs around USD 150. The hardware and the operation of the real-time application are summarized in the flowchart illustrated in Fig. 4.

The real-time control algorithm developed in the Arduino Uno works simply for both controllers designed. The angular position of the 2-RWP is read using the multi-turn potentiometer. The value read by the potentiometer is converted into an angle value, and also its derivatives are calculated in the script developed in the Arduino. In this way, the angular position, the angular velocity, and the angular acceleration of the pendulum are known for each iteration since they are necessary to evaluate the nonlinear control laws. The reaction wheels angular acceleration are the control signals provided by the control laws, and considering the pendulum angular acceleration, the desired motor torques can be evaluated as shown by equations (2) and (3).

It is essential to highlight some difficulties encountered in the plant. There are no encoders coupled to the DC motors. This means that the states related to the reaction wheels are unknown, and only the desired rates are commanded. Additionally, considering that $\frac{Ra}{K_t}$ is much greater than K_v and that the reaction wheels angular velocities are unknown, for the experimental application, equations (6) and (7) were considered as:

$$V_\alpha(t) = T_1\frac{R_a}{K_t} \tag{36}$$

$$V_\beta(t) = T_2\frac{R_a}{K_t} \tag{37}$$

After calculating the desired values of voltage for each DC motor, as shown by equations (36) and (37), these values are converted into PWM values ranging from -255 to 255. The relay module verifies which way the DC motors should rotate evaluating if these values are positive or negative that would indicate one way or the other one. Each PWM board is fed with an external power source, and it receives the controlled PWM signal from the Arduino. Thus, they can provide the correct and controlled voltage signal to the DC motors. After this point, the process is restarted. Moreover, a saturation limit of $|12|$ V is imposed on the voltage applied to both DC motors for both controllers designed in this paper. This limit does not affect the performance of the controllers, and it is imposed to protect the component. The flowchart depicted in Fig. 4 exemplifies how both controllers work. The desired and actual rates are compared, and the control laws are evaluated.

With the desired rates evaluated by the control laws, the reaction wheel motor torques are calculated so that the voltage of each reaction wheel can be evaluated. The voltages are converted into PWM values, and after the relay analysis which way the wheels must spin, they are commanded to the PWM boards. These boards combine the controlled signal with the external power supply to provide the correct

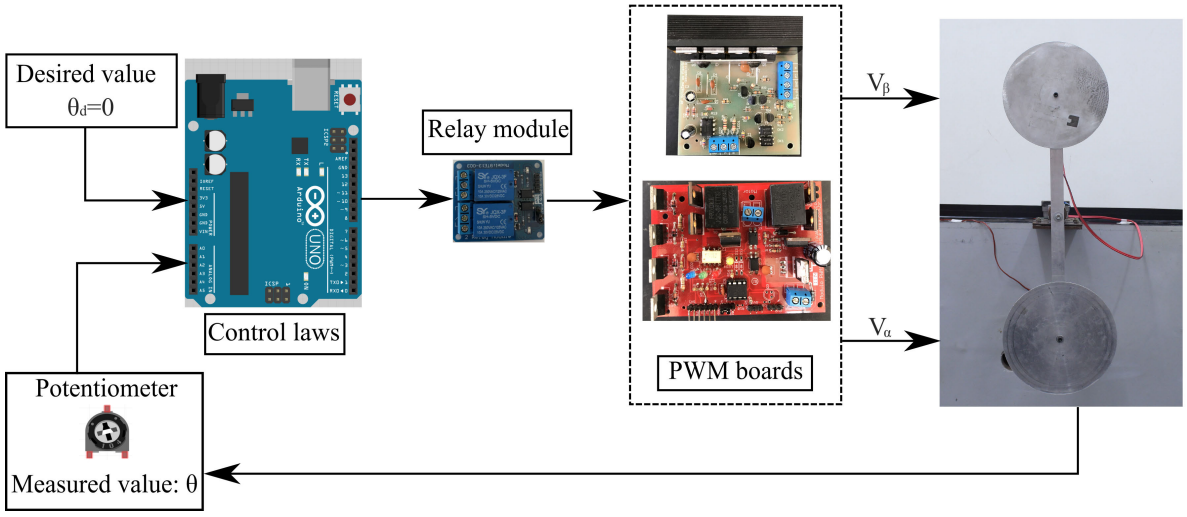

FIGURE 4. Flowchart of the real-time application.

voltage to the DC motors coupled to the reaction wheels. Subsequently, the angle value measured by the potentiometer is fed back, and the process is restarted.

VI. RESULTS

This section presents and compares the experimental results to drive and control an inverted pendulum using two reaction wheels considering the proposed control laws presented in equations (15) and (32). Additionally, Trentin *et al.* [13] designed a simple and well-known PID controller, and this result is compared with the two control techniques proposed in this paper. Fig. 5 depicts the controlled angular position for the 2-RWP for the three controllers where the sliding mode control technique exhibits a better performance reaching the equilibrium position first than the other controllers

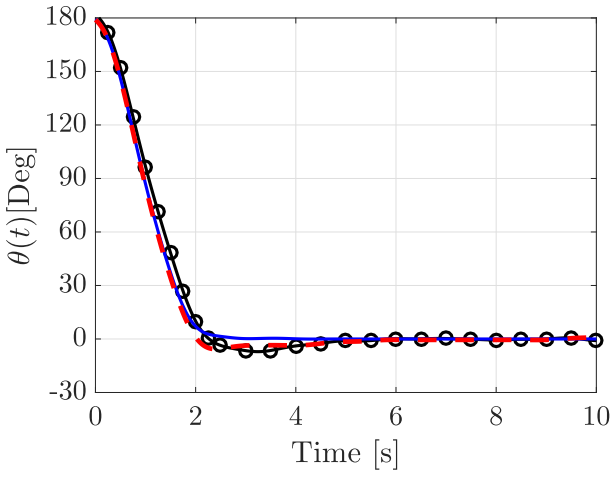

FIGURE 5. Comparison of the experimental pendulum angular position to drive and control the 2-RWP in the inverted position ($\theta = 0°$). - - - indicates nonlinear PD controller, ___ sliding mode controller, and -o- PID controller.

and presenting no overshoot. The SMC reached the inverted position in less than 3 seconds, while the other two controllers took around 5 seconds to drive and stabilize the pendulum in the inverted position. For the SMC, the gains used were $\eta = 10$ and $\gamma = 2$. The nonlinear proportional derivative controller has a smaller overshoot when compared to the PID controller. For this controller, the gains were $k_p = 60$ and $k_d = 15$.

Nevertheless, the experimental results are close, and a quantitative measure of performance can be helpful to evaluate it. One way to carry out this is to calculate performance indices. We evaluated two indices to verify if the same behavior is observed with different measures. Both indices used here are integrals evaluated over time. The first one, presented in equation (38), integrates the absolute error over time and does not weight the absolute error in the response [47].

$$\text{IAE} = \int_0^T |e(t)|dt \tag{38}$$

where $|e(t)|$ is the absolute error. The second, shown in (39), calculates the integral of the absolute error multiplied by time and weights the absolute error with time giving more importance for errors in regime [47].

$$\text{ITAE} = \int_0^T t|e(t)|dt \tag{39}$$

where t is time, $|e(t)|$ is the absolute error, and T is the total simulation time. The two indices analyze the response differently and are an alternative to quantitatively interpret the controller's performance since the goal of the control design here is to drive a pendulum using two reaction wheels to the inverted position (unstable equilibrium point) and keep it controlled there.

The values of the indices are presented in Table 1. Analyzing the values in Table 1, the nonlinear controllers had smaller indices than the PID, attesting better results of the nonlinear

TABLE 1. Performance indices for the experimental results.

Controller	IAE	ITAE
Sliding modes	3.2083	2.1256
Nonlinear proportional-derivative	3.3379	2.9042
PID	3.6902	3.2878

controllers, as seen in Fig. 5. The sliding mode control exhibited smaller indices than the nonlinear proportional-derivative controller. Nonetheless, taking into account that the sliding mode controller does not present overshoot and the pendulum reaches the inverted position faster than the nonlinear PD controller, the sliding mode controller outperforms the other controllers regarding the angular pendulum position.

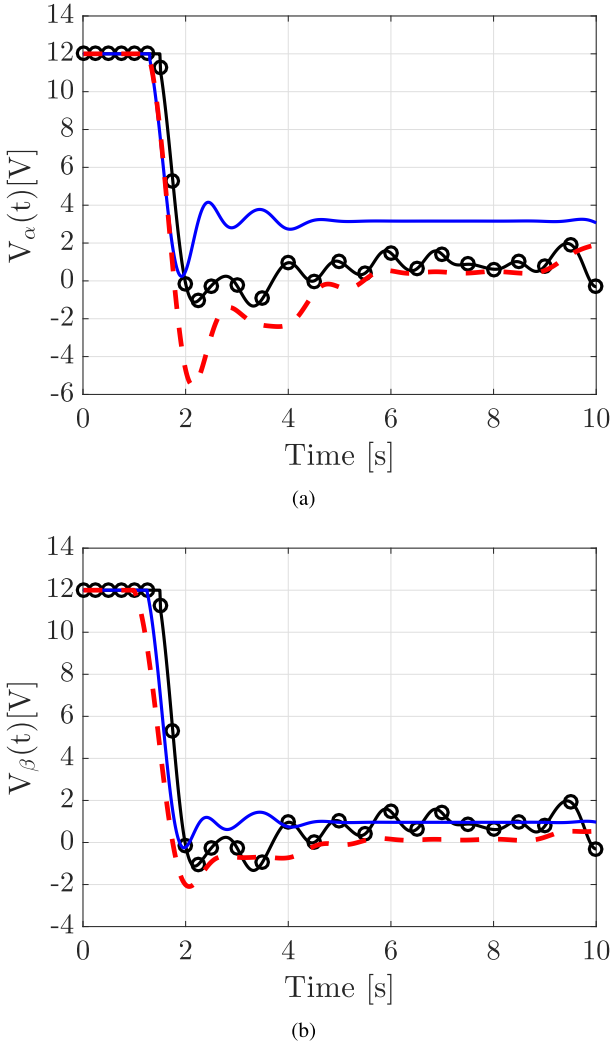

FIGURE 6. Comparison of the voltages applied to the DC motors of reaction wheels. - - - indicates nonlinear PD controller, ___ sliding mode controller, and -o- PID controller. (a) $V_\alpha(t)$ Voltage applied to DC motor of *reaction wheel 1* and (b) $V_\beta(t)$ Voltage applied to DC motor of *reaction wheel 2*.

Fig. 6 compares the voltages applied to the DC motors by each controller. By looking at the voltage applied to the DC motor of *reaction wheel 1*, Fig. 6a, the sliding mode controller presents a higher value of voltage, while in steady-state, the voltage applied by the nonlinear proportional derivative controller and PID are very close. However, when analyzing the voltage applied to the DC motor of *reaction wheel 2*, charted in Fig. 6b , the values for all three controllers are very close. Thus, to a better evaluation of these results, the root means square (RMS) value of the voltages were calculated, and they are presented in Table 2.

TABLE 2. Root mean square values of the voltages applied to the DC motors.

Controller	RMS ($V_\alpha(t)$)	RMS ($V_\beta(t)$)
Sliding modes	5.4235	4.6609
Nonlinear proportional-derivative	4.8650	4.3569
PID	4.9391	4.9391

The RMS values of the nonlinear proportional-derivative controller are the smaller ones, which indicates that this controller has smaller energy consumption. When we evaluate the RMS values for the voltage applied to DC motor 2, the PID controller had the highest value. The RMS of all the voltage control signals were calculated for 10 seconds.

Analyzing the RMS values of the *reaction wheel 1*, we note that the sliding mode controller had the highest value. For the better performance of the sliding mode controller, it is necessary to spend more energy. Nonetheless, it is essential to observe that the control signal for the SMC is much more steady, and it outperforms the other controllers tested. This is possible due to the SMC low sensitivity to the noise presented in the real-time measurements, whereas the other two controllers present much more oscillatory control voltage signals. When the sliding function is reached (as seen in Fig. 8 approximately at 2 seconds), one of the main features of sliding mode control is to maintain the system's behavior under the minimum influence of parametric uncertainties and external disturbances. When this occurs, the system behaves with the designed dynamic characteristics given by equation (21), with $\sigma(e, t) = 0$, providing robustness to the system and a much more steady control signal.

However, one of the reasons for the high voltage values can be the nonlinear behavior of the friction encountered in the self-manufactured plant. After the pendulum is controlled in the inverted position, its angular velocity is almost zero. Thus, the Coulomb friction component has a more significant contribution and the controller has to deal with this. The voltages values should be closer to zero or around zero, but due to the friction, a higher voltage value is commanded for *reaction wheel 1* when using the sliding mode control. It would be interesting to develop a control strategy that can reduce the voltage after the pendulum is controlled in the inverted position or a better manufactured experimental device could be built where the friction encountered can be minimized.

Figures 7 and 8 present specific results of the sliding mode controller. Fig. 7 exhibits the designed sliding function in the error configuration space where the numerical and

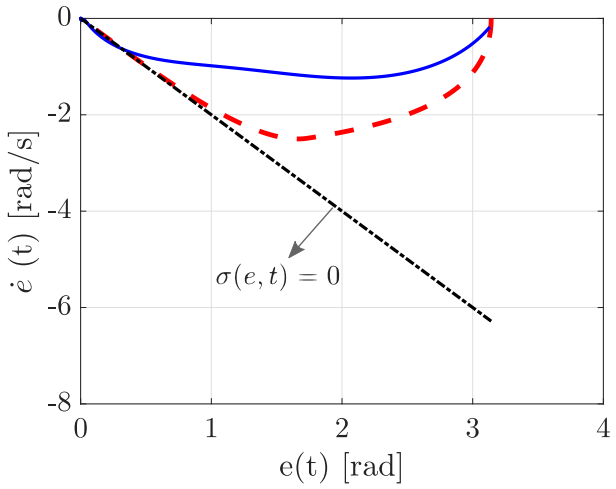

FIGURE 7. Error configuration space with desired sliding function. - - - indicates numerical result, ___ the experimental result and -•- the desired sliding function.

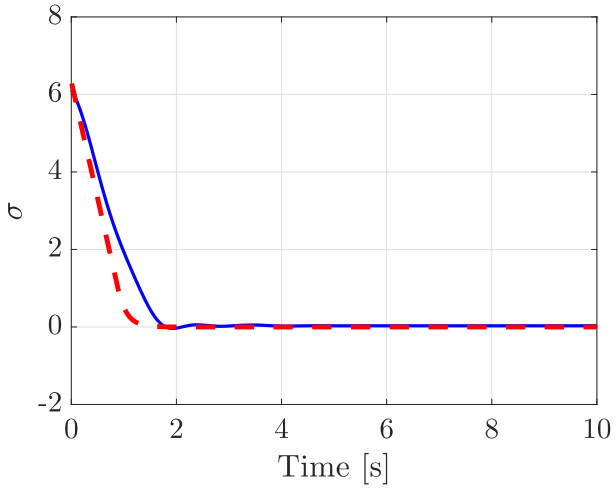

FIGURE 8. Sliding function to control the 2-RWP in the inverted position ($\theta = 0°$). - - - indicates numerical result and ___ the experimental result.

experimental results for the controller can reach the function and slide to the equilibrium position. For a better evaluation of the experimental results, the numerical ones were not presented in figures 5 and 6. Nonetheless, for the specific analysis of the VSC, the numerical results are compared to the experimental ones. The numerical simulations were carried out before the real-time experiments to ensure that the proposed control laws were suitable to drive and control an inverted pendulum with two reaction wheels.

In the algorithm developed for the numerical simulations, the desired and actual rates are compared, and the control laws, presented in (15) and (32), are evaluated. With the desired rates evaluated by the control laws, the reaction wheel motor torques, shown in (2) and (3), are calculated, since they are necessary for the complete integration of the mathematical model of the 2-RWP, composed by the equation of motion presented in (9) and both motor torques equations. The numerical integration is done using a fourth-order Runge-Kutta method with a time step of 0.001 s. The resulting rates of the integration process are fed back, and the process is restarted.

Fig. 8 depicts the behavior of the sliding function ($\sigma(e, t)$). When it is zero, it means that the system has reached the sliding function designed in equation (21). If the function remains at zero, it shows that the system is sliding. The system will thereby slide to the equilibrium point, describing the property of attractiveness, which is also one of the features of the sliding mode control. The reachability and the attractiveness properties are proven by analyzing the numerical and experimental results presented in Figures 7 and 8.

The control law proposed can take the system to the sliding function and keep it there controlled. Furthermore, it is common in any control design to find discrepancies between the model and the real-time experiment because of unmodeled dynamics, parameter uncertainties, and the presence of external disturbances [12], [20].

Furthermore, both nonlinear controllers designed can be applied for any initial conditions. Additionally, the controllers can also track the desired trajectory. The function for the desired trajectory (θ_d) and its rates have to be provided as input to the controllers. Thereby, it is also possible for the controllers designed to track the desired trajectory. Moreover, it is recommended that the pendulum with two reaction wheels be controlled in the inverted position or to track the desired trajectory. If a set-point that is not an equilibrium point is desired, the torque caused by gravity is not zero, and it is also added. Thus, the controller will have to deal with the friction and the torque caused by gravity. Thereby, a higher voltage signal than the one employed to control the pendulum in the inverted position will have to be applied to the DC motors, and in steady-state, this value tends to increase until the saturation limit is reached. Thus, after some time, the DC motors' saturation limits can be reached, or the reaction wheels will reach very high angular velocities, which can cause a catastrophic failure to the system. Either way, this system will no longer be able to be controlled in that position. Additionally, the following link allows the reader to see the performance of the real-time controller implemented: https://youtu.be/HbPgJYSusmc

VII. CONCLUSION

The main contribution of this paper was to show the application and comparison of two nonlinear control techniques to drive and control an inverted pendulum using a new type of actuator involving two reaction wheels. This different configuration of an inverted pendulum can be further explored to test new controllers, for example, to track the desired trajectory instead of controlling the pendulum in the inverted position. Furthermore, swing-up control strategies using one or both reaction wheels can also be tested. In this paper, the design and proof of the stability of a nonlinear proportional-derivative controller and a sliding mode controller were carried out. Additionally, the use of low-cost

hardware to reproduce these controllers in a real-time application has proven to be very efficient despite the difficulties encountered.

The strategies presented adequate experimental results, which were much better than the previous one using a simple PID controller. The performance indices quantitatively measured this improvement. The sliding mode control had a more reliable performance when compared to the nonlinear proportional-derivative, confirming that the use of a technique that deals with model uncertainty provides a better outcome. When analyzing the voltage applied to the DC motors to control the inverted pendulum, we found that the values were higher than the expected. These values for a perfect inverted pendulum system controlled in an equilibrium point should be zero. In real-time experiments, it is expected that these values be close to zero or around zero. One possible reason might be due to the presence of the Coulomb friction encountered when identifying the friction of the experimental device. For future work, a control strategy to decrease the voltage values and bring them as close as possible to zero will be carried out.

REFERENCES

[1] M. W. Spong, P. Corke, and R. Lozano, "Nonlinear control of the reaction wheel pendulum," *Automatica*, vol. 37, no. 11, pp. 1845–1851, Nov. 2001.

[2] F. Grasser, A. D'Arrigo, S. Colombi, and A. C. Rufer, "JOE: A mobile, inverted pendulum," *IEEE Trans. Ind. Electron.*, vol. 49, no. 1, pp. 107–114, 2002.

[3] K. Furuta, "Control of pendulum: From super mechano-system to human adaptive mechatronics," in *Proc. 42nd IEEE Int. Conf. Decis. Control*, vol. 2, Dec. 2003, pp. 1498–1507.

[4] M. Yue and X. Wei, "Dynamic balance and motion control for wheeled inverted pendulum vehicle via hierarchical sliding mode approach," *Proc. Inst. Mech. Eng., I, J. Syst. Control Eng.*, vol. 228, no. 6, pp. 351–358, Jul. 2014.

[5] J. F. S. Trentin, S. da Silva, and H. Schaub, "Variable speed control moment gyroscope in an inverted pendulum," *J. Dyn. Syst., Meas., Control*, vol. 141, no. 11, Nov. 2019, Art. no. 111012.

[6] A. Owczarkowski, D. Horla, and J. Zietkiewicz, "Introduction of feedback linearization to robust LQR and LQI control—Analysis of results from an unmanned bicycle robot with reaction wheel," *Asian J. Control*, vol. 21, no. 2, pp. 1028–1040, Mar. 2019.

[7] H. Jin, T. Wang, F. Yu, Y. Zhu, J. Zhao, and J. Lee, "Unicycle robot stabilized by the effect of gyroscopic precession and its control realization based on centrifugal force compensation," *IEEE/ASME Trans. Mechatronics*, vol. 21, no. 6, pp. 2737–2745, Dec. 2016.

[8] G. P. Neves, B. A. Angélico, and C. M. Agulhari, "Robust H2 controller with parametric uncertainties applied to a reaction wheel unicycle," *Int. J. Control*, vol. 0, no. 0, pp. 1–11, 2019.

[9] C. Cai, J. Lu, and Z. Li, "Kinematic analysis and control algorithm for the ballbot," *IEEE Access*, vol. 7, pp. 38314–38321, 2019.

[10] F. H. B. Lima, E. Poleze, G. P. das Neves, and B. A. Angelico, "LMI based robust H2 control of a ball balancing robot with omni-wheels," in *Proc. 18th Eur. Control Conf. (ECC)*, Jun. 2019, pp. 2090–2095.

[11] N. R. Sekhar, M. Korrapati, R. Hota, and C. S. Kumar, "New dynamic model and simulation of the ballbot using reaction wheels," in *Machines, Mechanism and Robotics*, D. N. Badodkar and T. A. Dwarakanath, Eds. Singapore: Springer, 2019, pp. 807–816.

[12] Y. Liu and H. Yu, "A survey of underactuated mechanical systems," *IET Control Theory Appl.*, vol. 7, no. 7, pp. 921–935, May 2013.

[13] J. F. S. Trentin, T. P. Cenale, S. da Silva, and J. M. D. S. Ribeiro, "Attitude control of inverted pendulums using reaction wheels: Comparison between using one and two actuators," *Proc. Inst. Mech. Eng., I, J. Syst. Control Eng.*, vol. 234, no. 3, pp. 420–429, Mar. 2020.

[14] C. A. Ibañez, O. G. Frias, and M. S. Castañón, "Lyapunov-based controller for the inverted pendulum cart system," *Nonlinear Dyn.*, vol. 40, no. 4, pp. 367–374, Jun. 2005.

[15] C. A. Ibáñez and J. H. S. Azuela, "Stabilization of the furuta pendulum based on a Lyapunov function," *Nonlinear Dyn.*, vol. 49, nos. 1–2, pp. 1–8, May 2007.

[16] M. de Queiroz, D. Dawson, S. Nagarkatti, and F. Zhang, *Lyapunov-Based Control of Mechanical Systems* (Control Engineering). Boston, MA, USA: Birkhäuser, 2012.

[17] H. Schaub and J. L. Junkins, *Analytical Mechanics of Space Systems*, 3rd ed. Reston, VA, USA: AIAA Education Series, 2014.

[18] J. Slotine and W. Li, *Applied Nonlinear Control*. Upper Saddle River, NJ, USA: Prentice-Hall, 1991.

[19] M. López-Martínez, J. Á. Acosta, and J. M. Cano, "Non-linear sliding mode surfaces for a class of underactuated mechanical systems," *IET Control Theory Appl.*, vol. 4, no. 10, pp. 2195–2204, Oct. 2010.

[20] J. Liu and X. Wang, *Advanced Sliding Mode Control for Mechanical Systems: Design, Analysis and MATLAB Simulation*. Berlin, Germany: Springer, 2012.

[21] V. I. Utkin, *Sliding Modes and Their Applications in Variable Structure Systems*. Moscow, Russia: MIR, 1978.

[22] D. Zhao, H. Hu, T. Bai, Y. Bai, X. Liang, and Y. Wang, "Variable structure control for uncertain system," in *Proc. 36th Chin. Control Conf. (CCC)*, Jul. 2017, pp. 3691–3696.

[23] R. A. DeCarlo, S. H. Zak, and G. P. Matthews, "Variable structure control of nonlinear multivariable systems: A tutorial," *Proc. IEEE*, vol. 76, no. 3, pp. 212–232, Mar. 1988.

[24] J. P. F. Garcia, J. M. S. Ribeiro, E. S. Martins, and J. J. F. Silva, "Continuous-time and discrete-time sliding mode control accomplished using a computer," *IEE Proc. Control Theory Appl.*, vol. 152, no. 2, pp. 220–228, Mar. 2005.

[25] H.-P. Ren and J. Hu, "Nonlinear integral sliding mode variable structure control for two-tank system with input-limitation," in *Proc. 43rd Annu. Conf. IEEE Ind. Electron. Soc. (IECON)*, Oct. 2017, pp. 5150–5155.

[26] J. Wei, K. Liu, and G. Radice, "Modified nonlinear integral sliding mode control for satellite attitude stabilization using magnetically suspended gimbaled momentum wheel," in *Proc. IEEE Int. Conf. Inf. Autom.*, Aug. 2015, pp. 1473–1478.

[27] Q. Hu, "Robust adaptive sliding-mode fault-tolerant control with L2-gain performance for flexible spacecraft using redundant reaction wheels," *IET Control Theory Appl.*, vol. 4, no. 6, pp. 1055–1070, Jun. 2010.

[28] F.-K. Yeh, "Sliding-mode adaptive attitude controller design for spacecrafts with thrusters," *IET Control Theory Appl.*, vol. 4, no. 7, pp. 1254–1264, Jul. 2010.

[29] P. Zhang, J. Qiao, L. Guo, and W. Li, "Sliding mode friction observer based control for flexible spacecraft with reaction wheel," *IET Control Theory Appl.*, vol. 11, no. 8, pp. 1274–1281, May 2017.

[30] Z. Song, C. Duan, H. Su, and J. Hu, "Full-order sliding mode control for finite-time attitude tracking of rigid spacecraft," *IET Control Theory Appl.*, vol. 12, no. 8, pp. 1086–1094, May 2018.

[31] R. Mondai and M. M. Rahman, "Dynamic analysis of variable structure based sliding mode intelligent load frequency control of interconnected nonlinear conventional and renewable power system," in *Proc. Int. Conf. Intell. Comput., Instrum. Control Technol. (ICICICT)*, Jul. 2017, pp. 393–400.

[32] Q. H. Ngo and K.-S. Hong, "Adaptive sliding mode control of container cranes," *IET Control Theory Appl.*, vol. 6, no. 5, pp. 662–668, 2012.

[33] L. A. Tuan and S.-G. Lee, "Sliding mode controls of double-pendulum crane systems," *J. Mech. Sci. Technol.*, vol. 27, no. 6, pp. 1863–1873, Jun. 2013.

[34] C. Izaguirre-Espinosa, V. Parra-Vega, P. Castillo, A. J. Muñoz-Vázquez, and A. Sánchez-Orta, "Attitude control of quadrotors based on fractional sliding modes: Theory and experiments," *IET Control Theory Appl.*, vol. 10, no. 7, pp. 825–832, Apr. 2016.

[35] F. F. Ardakani, H. E. Ardekani, K. H. Boozanjani, S. Taghvaei, and S. A. Haghpanah, "Fuzzy sliding mode control of a bio-inspired exoskeleton robot in pick and place task with obstacle avoidance," in *Proc. IEEE 4th Int. Conf. Knowl.-Based Eng. Innov. (KBEI)*, Dec. 2017, pp. 0459–0464.

[36] J. Huang, Z.-H. Guan, T. Matsuno, T. Fukuda, and K. Sekiyama, "Sliding-mode velocity control of mobile-wheeled inverted-pendulum systems," *IEEE Trans. Robot.*, vol. 26, no. 4, pp. 750–758, Aug. 2010.

[37] M. Rubagotti, A. Ferrara, and M. L. D. Vedova, "Time-optimal sliding-mode control of a mobile robot in a dynamic environment," *IET Control Theory Appl.*, vol. 5, no. 16, pp. 1916–1924, Nov. 2011.

[38] S. Riachy, Y. Orlov, T. Floquet, R. Santiesteban, and J.-P. Richard, "Second-order sliding mode control of underactuated mechanical systems I: Local stabilization with application to an inverted pendulum," *Int. J. Robust Nonlinear Control*, vol. 18, nos. 4–5, pp. 529–543, Mar. 2008.
[39] J.-J. Wang, "Stabilization and tracking control of X–Z inverted pendulum with sliding-mode control," *ISA Trans.*, vol. 51, no. 6, pp. 763–770, Nov. 2012.
[40] R. Iriarte, L. T. Aguilar, and L. Fridman, "Second order sliding mode tracking controller for inertia wheel pendulum," *J. Franklin Inst.*, vol. 350, no. 1, pp. 92–106, 2013.
[41] N. Adhikary and C. Mahanta, "Integral backstepping sliding mode control for underactuated systems: Swing-up and stabilization of the Cart–Pendulum system," *ISA Trans.*, vol. 52, no. 6, pp. 870–880, Nov. 2013.
[42] Z.-Q. Guo, J.-X. Xu, and T. H. Lee, "Design and implementation of a new sliding mode controller on an underactuated wheeled inverted pendulum," *J. Franklin Inst.*, vol. 351, no. 4, pp. 2261–2282, Apr. 2014.
[43] R. Kelly and J. Llamas, "Determination of viscous and Coulomb friction by using velocity responses to torque ramp inputs," in *Proc. IEEE Int. Conf. Robot. Autom.*, vol. 3, May 1999, pp. 1740–1745.
[44] R. Mukherjee and D. Chen, "Asymptotic stability theorem for autonomous systems," *J. Guid., Control, Dyn.*, vol. 16, no. 5, pp. 961–963, Sep. 1993.
[45] R. Mukherjee and J. L. Junkins, "Invariant set analysis of the hub-appendage problem," *J. Guid., Control, Dyn.*, vol. 16, no. 6, pp. 1191–1193, Nov. 1993.
[46] J. L. Junkins and Y. Kim, *Introduction to Dynamics and Control of Flexible Structures*. Reston, VA, USA: American Institute of Aeronautics and Astronautics, 1993.
[47] R. C. Dorf and R. H. Bishop, *Modern Control Systems*. London, U.K.: Pearson, 2011.

JOÃO FRANCISCO SILVA TRENTIN received the B.Sc. degree in mechanical engineering from Universidade Estadual Paulista (UNESP), Ilha Solteira, Brazil, in 2016, where he is currently pursuing the Ph.D. degree. His research interests include nonlinear dynamics, linear and nonlinear control, and inverted pendulum-like systems.

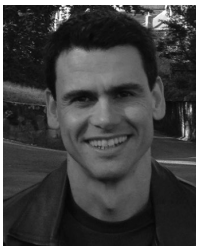

SAMUEL DA SILVA received the B.Sc. and M.Sc. degrees in mechanical engineering from Universidade Estadual Paulista (UNESP), Ilha Solteira, Brazil, in 2002 and 2005, respectively, and the D.Sc. degree in mechanical engineering from the State University of Campinas (UNICAMP), in 2008. He was a Visiting Researcher at Arts et Métiers ParisTech (ENSAM) with a fellowship from the São Paulo Research Foundation (FAPESP), in 2019. He is currently an Associate Professor with the Department of Mechanical Engineering, UNESP, and also a Research Fellow of the National Council for Scientific and Technological Development (CNPq). His research interests include system identification, signal processing, nonlinear vibrations, structural health monitoring, and applied mechanics.

JEAN MARCOS DE SOUZA RIBEIRO received the B.Sc., M.Sc., and D.Sc. degrees in electrical engineering from Universidade Estadual Paulista (UNESP), Ilha Solteira, Brazil, in 1998, 2001, and 2006, respectively. He is currently an Assistant Professor with the Department of Electrical Engineering, UNESP. His research interests include control theory and its applications, variable structure control, sliding modes control, and the control and electronic drive of electrical machines.

HANSPETER SCHAUB is the Glenn L. Murphy Chair of engineering with the University of Colorado Boulder and is the current Graduate Chair of the Department of Aerospace Engineering Sciences. He has over 20 years of research experience, of which four years at Sandia National Laboratories. His research has led to about 164 journals and 261 conference publications, as well as a fourth edition of the textbook *Analytical Mechanics of Space Systems*. His research interests are in nonlinear dynamics and control, astrodynamics, relative motion dynamics, and relative motion sensing. In the last decade, he has developed the emerging field of charged astrodynamics. He has been the ADCS Lead of the CICERO Mission and the ADCS Algorithm Lead of the Mars Mission. He is a Fellow of the AIAA and AAS, and has won the AIAA/ASEE Atwood Educator Award and the AIAA Mechanics and Control of Flight Award. He has been awarded the H. Joseph Smead Faculty Fellowship, the Provosts Faculty Achievement Award, the Faculty Assembly Award for Excellence in Teaching, and the Outstanding Faculty Advisor Award. He currently serves as the Editor-in-Chief for the AIAA *Journal of Spacecraft and Rockets*.